AIAA JOURNAL
Vol. 42, No. 7, July 2004

# Behavior of Turbulence Flowing Through a Compressor Cascade

Diego H. de la Riva,* William J. Devenport,† and Chittiappa Muthanna‡
*Virginia Polytechnic Institute and State University, Blacksburg, Virginia 24061*
and
Stewart A. L. Glegg§
*Florida Atlantic University, Dania Beach, Florida 33004*

**The behavior of grid turbulence flowing through a compressor cascade has been measured and compared with basic predictions using rapid distortion theory (RDT). The cascade, operated at a chord Reynolds number of $3.8 \times 10^5$, produces a turning of 11.8 deg. The inflow turbulence had an intensity of 3.1%, a longitudinal integral scale equivalent to 26% of the upstream projected blade spacing, and spectral and correlation properties consistent with the expectations of homogeneous isotropic turbulence. Near the passage center, the freestream decay of turbulence stresses and spectra is substantially modified by the deceleration and turning of the flow. Near the blades, the turbulence is additionally modified by the blocking of normal velocity fluctuations. Overall, we find the evolution of turbulence through the cascade, including its spectrum and space time correlations, to be quantitatively consistent with RDT effects superimposed over a background of viscous decay. This suggests that, at least in circumstances similar to those modeled here, RDT may offer a viable approach for the calculation of the modification of turbulence passing through a blade row.**

## Introduction

CONSIDER turbulence encountering a row of blades, such as the rotor or stator of a turbomachine. The turbulence flows past the blades that distort it and add their own wakes. The combined flow then impinges on a second set of blades. The interaction of the turbulence with both blade rows will generate noise and vibration. To predict these, it is necessary to have an estimate of the intensity, spectrum, and two-point space–time correlation of the turbulence as it enters each blade row.

In many situations, such as when the turbulence forms part of an unmodified thick vehicle boundary layer or the circumferential average of a series of wake flows, existing approximate techniques may be used to estimate the spectral character of the turbulence entering the first blade row.[1–3] At least, they should capture the main features of the turbulence. However, this is not the case for the second blade row because the turbulence it sees is likely to have been heavily modified by its distortion in the first blade row. This is particularly true when the initial turbulence is slowly evolving and of large scale, such as when it is ambient or associated with boundary-layer growth along the entire length of a vehicle.

Because spectra and correlations are required, conventional computational fluid dynamics, (CFD) is of limited use in this problem. Although such quantities could be obtained from large-eddy simulation (LES) or direct numerical simulation (DNS), most realistic configurations are far too complex and of too high a Reynolds number to be modeled in this way. An alternative approach is to use rapid distortion theory (RDT), in which the linearized equations of motion are solved. RDT can, in principle, provide predictions of spectral and correlation functions provided certain requirements are met.

Received 13 June 2003; revision received 30 January 2004; accepted for publication 1 March 2004. 

*Graduate Assistant, Department of Mechanical Engineering. Student Member AIAA.
†Professor, Department of Aerospace and Ocean Engineering, 215 Randolph Hall. Senior Member AIAA.
‡Graduate Assistant, Department of Aerospace and Ocean Engineering, 215 Randolph Hall; currently Research Associate, Laboratory for Aero and Hydrodynamics, Delft University, Leeghwaterstraat 21, 2628 CA Delft, The Netherlands. Member AIAA.
§Professor, Ocean Engineering Department. Senior Member AIAA.

Much of RDT stems from the pioneering work of Batchelor and Proudman.[4] They showed how Cauchy's equation, expressing the transport of vorticity by a mean flow field, can be used to predict the velocity wave number spectrum of homogeneous turbulence undergoing homogeneous distortion, given the assumptions of RDT. Later, Hunt[5] extended this theory to include mean-flow inhomogeneity and the effects of the nonpenetration condition at solid surface boundaries. In RDT, the nonpenetration condition does not alter the vorticity transport, but it sets up an additional irrotational velocity field that cancels the wall-normal component of the rotational velocity at the surface. The irrotational field has a large influence on turbulence intensities and correlations measured in the vicinity of the surface (effects sometimes referred to as blade blocking). Furthermore, it is associated with the unsteady surface pressure field. For this second reason, RDT has been heavily developed as a tool for hydro/aeroacoustic predictions of rotor- or stator-generated noise. For example, RDT prediction methods for sound generation and propagation have been developed for isolated airfoils, linear cascades, and annular cascades for both irrotational and swirling mean flowfields.[6–14]

Much less attention has been paid to the use of RDT as a means for explicit prediction of the evolution of the turbulence space–time correlations through a blade row. Graham,[15] following Hunt and Graham[16] and Kullar and Graham,[17] developed explicit expressions for the effects of an unswept cascade of flat plates at zero angle of attack and small separation on a homogeneous turbulent field. In this situation there is no mean flow distortion, and so all effects are generated by blade surface blocking. Graham found that RDT predicted quite well the suppression of fluctuations in the wall-normal component of velocity, but that there were significant differences in tangential velocity fluctuations and spectra, which were found to be very sensitive to plate separation. Some of the differences were attributed to the nonuniform strains experienced by the turbulence near the plate leading edges (which were not modeled) and some nonlinear evolution of the turbulence in the experiment. Graham also considered the situation where the turbulence passed over a single flat plate, and he observed similar results. Outside the boundary layer, this situation is analogous to that produced by the interaction of initially homogeneous turbulence with a suddenly introduced plane wall, or free surface, which has been modeled both numerically and experimentally by a number of researchers.[18–22] Of particular interest here is the insight of Perot and Moin[20] who, following Hunt,[23] show that RDT can only model the initial influence of the new boundary condition on the turbulence and not its subsequent evolution. In the turbomachinery problem, this implies

that RDT may only simulate the effects of the blade blocking in the leading-edge regions, or when the turbulence scale is very large. However, several of these studies show that RDT actually provides reasonable predictions, particularly of the wall-normal velocity fluctuations, over a significantly greater period than this. This can be thought of as coincidental[20,22] because it appears that the influence of the nonlinear terms in the equations of motion should be significant over such an extended period. Alternatively, as discussed by Kevlahan and Hunt,[24] it may be that the nonlinear terms are inhibited, particularly in the presence of weak straining. This may explain why some classic experimental measurements of distorting turbulence, for example, that in Ref. 25, are fairly accurately described by RDT, even though the period of distortion is much longer than that over which RDT should be valid.[24]

This, coupled with the fact that RDT appears to be the only choice for prediction in the turbomachinery situation, suggest that experimental data detailing the actual distortion and blade blocking effects produced by a realistic blade row are needed. However, little or no two-point experimental data are available for such situations, and those single-point measurements that are available are not well suited for detailed comparison with the predictions or hypotheses of RDT. (Perhaps the most useful are those presented by Graham,[15] which include only single-point profiles measured downstream of an unstaggered cascade of flat plates.)

This is not to say that experimental work in the influence of freestream turbulence on turbomachinery is lacking. There is a large body of literature devoted to turbulence effects on heat transfer and boundary-layer transition in turbines and turbine cascades because of its relevance to flows downstream of combustors.[26–30] Only few studies, however, have included turbulence measurements[31–35] and only Bangert et al.[34] and Ames and Plesniak[35] clearly documented the evolution freestream turbulent field as it convects through the blade row. The details of these experiments make them of limited relevance here. (Ames and Plesniak generated nonhomogeneous turbulence using a mock combustor, Bangert et al. examined rapidly decaying freestream turbulence and made measurements only away from the blade surfaces.) However, these studies do show evidence of important RDT-type effects: the reduction in streamwise turbulence intensity and increase in length scale as the flow is accelerated through the cascade[34] and the reduction in the intensity of the wall-normal velocity fluctuations in the vicinity of the blades.[35]

With the aforementioned backdrop, the objective of our study is to provide the experimental information needed to evaluate the suitability of RDT as it currently stands 1) for prediction of the evolution of space–time structure of turbulence passing through a propulsor or stator and 2) to provide a basis for improvements in the theory.

To achieve this goal, we have made detailed measurements documenting the evolution of grid turbulence as it convects through a linear cascade that contains many of the features (blade thickness, flow curvature and deceleration, tip leakage) found in an actual rotor. These measurements have been compared with basic RDT predictions of the effects of the flow distortion and blade blocking on the turbulence. Comparison with these predictions enables blade blocking and nonlinear effects to be more easily identified in the data. More details of this study are described by de la Riva[36] and Muthanna.[37]

## Apparatus and Instrumentation

Measurements were made in the Virginia Polytechnic and State University Fan Cascade Wind Tunnel (Fig. 1). The facility contains an eight-blade, seven-passage linear cascade with 4.3%-thick General Electric (GE) rotor B compressor blades, each with a 254-mm chord, and an aspect ratio of 1 (Fig. 2). The blades are mounted with the tip gap to the lower endwall set at 4.2 mm, a stagger angle of 56.9 deg, an inlet angle of 65.1 deg, and a blade spacing of 236 mm in a section 254 mm in height. Blade coordinates are given by Wang.[38] Boundary layers on both sides of the blades were tripped by the use of distributed roughness strips placed 25.4 mm downstream of the blade leading edges.

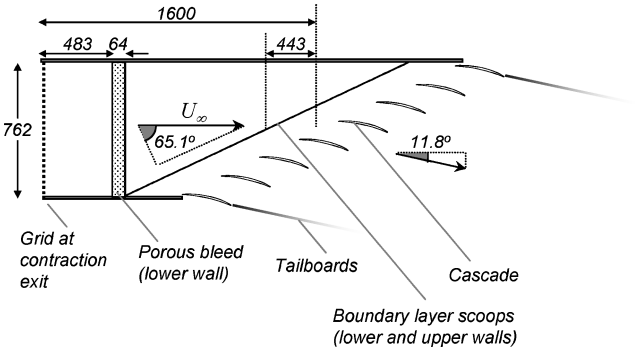


**Fig. 1 Plan view schematic of the cascade wind tunnel; dimensions in millimeters.**

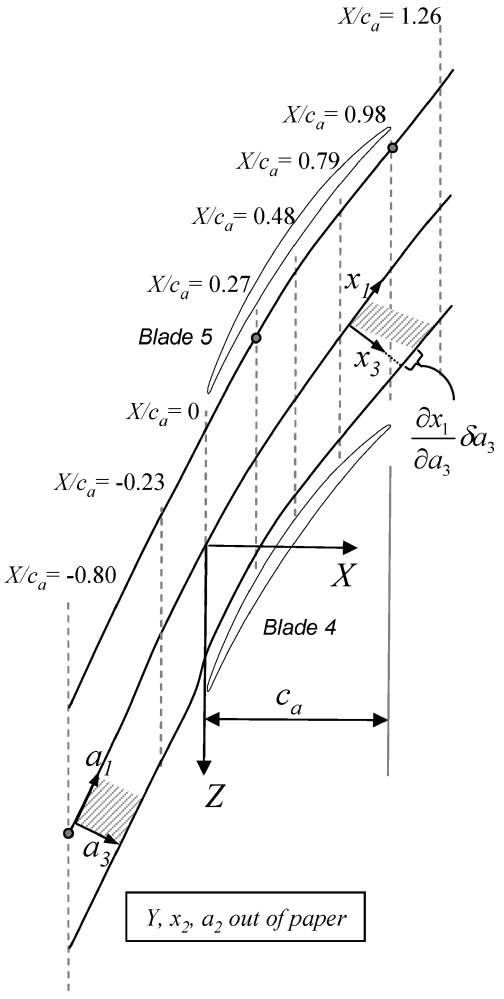


**Fig. 2 Detail showing the central blade passage: ——, integrated from the measured mean velocity field and ●, anchor points for two-point spanwise measurements presented in Figs. 4 and 15.**

The facility is powered by a 15-hp centrifugal blower that supplies air to a settling chamber terminated by a 6.43:1 two-dimensional contraction. A rectangular duct, 305 mm high × 762 mm wide, guides flow from the contraction exit onto the cascade, the distance between the two being 1600 mm at the tunnel centerline. Boundary layers on the 762-mm-wide upper and lower walls are removed before reaching the cascade by the use of 25.4-mm-high boundary-layer scoops. New pitchwise-uniform endwall boundary layers grow from the scoops over a streamwise distance of some 443 mm before reaching the leading-edge line of the cascade, that is, an axial distance of 186.7 mm. Boundary-layer thickness just upstream of the cascade entrance is about 13 mm (Ref. 37).

This facility is the same as that used for the earlier studies of Muthanna and Devenport,[39] Wang and Devenport,[40] and Wenger

et al.,[41] except that the distance between the boundary-layer scoops and cascade was increased for the present study, by movement of the latter 200 mm downstream. In addition, a lateral strip of the lower wind-tunnel wall, 483 mm downstream of the cascade exit, was replaced with a porous plate. The plate was designed to bleed some 8% of the test-section mass flow, reducing the size of the boundary layer that needed to be removed by the lower endwall boundary-layer scoop. Once reconfigured, the facility was recalibrated: The boundary-layer scoops and tailboard angles were readjusted to eliminate streamwise pressure gradient across the scoops and net pitchwise pressure gradient upstream and downstream of the cascade. After calibration, the turning angle of the facility was found to be 11.8 deg, this being slightly less than the 12.5 deg measured for the earlier configuration.

For most of the measurements in this paper, a turbulence-generating grid was placed in the flow approaching the cascade. The grid consists of 10 vertical and 4 horizontal round steel rods, each of diameter 15.9 mm, welded together in a biplanar mesh of cell size 74.9 mm with the horizontal rods downstream of the vertical rods. The open-area ratio of the grid is 62%. The grid was placed at the contraction exit with its center at a distance of 1600 mm (20 grid cells) upstream of the center of the leading-edge line of the cascade (Fig. 1). The grid was mounted perpendicular to the flow, instead of being staggered with the cascade, because a staggered grid would turn the flow approaching the cascade, upsetting the facility calibration. Turbulence generated by the grid passed over the porous bleed plate and between the boundary-layer scoops before reaching the cascade.

Single- and two-point velocity and turbulence measurements were made with miniature four-sensor hot-wire probes manufactured by Auspex Corp. (Type AVOP 4 100). These probes have two orthogonal X wire arrays of sensors within a total measurement volume of approximately 0.5 $mm^3$. Each sensor was operated separately by the use of a Dantec 56C17/56C01 constant temperature anemometer unit. Hot-wire signals were buffered by four buck and gain amplifiers containing calibrated resistance–capacitance (RC) filters to limit their frequency response to 50 kHz. Signals were sampled via a 16-bit Hewlett–Packard E1406A digitizer and recorded on an IBM compatible computer.

Probes were calibrated for velocity before and after each measurement run by their placement in the uniform jet of a TSI calibrator and the use of King's law to correlate the wire output voltages with the cooling velocities. Velocity components were determined from the cooling velocities by means of a direct angle calibration (see Wittmer et al.[42]). Hot-wire signals were corrected for ambient temperature drift via the method of Bearman.[43] The frequency response of each sensor/anemometer bridge combination was calibrated by direct measurement of its impulse response, simulated by the direction of a pulsed YAG laser at the sensor. Phase and amplitude characteristics for all of the sensor channels were to frequencies in excess of 30 kHz. The accuracy of this system for mean velocity and turbulence measurements has been established through measurements taken in a fully developed turbulent pipe flow.[42]

A computer-controlled three-axis traverse system was used to position the probes. Each axis was driven by a stepper motor (Compumotor Model S75-83-MO) and controlled by a PDX13 single-axis packaged ministep drive. The resolution of the programmable traverse movement was 0.025 mm. Probes were supported by the use of a 9.5-mm-diam stem held by the traverse and introduced to the flow in the spanwise direction through the upper endwall. Probes were held aligned approximately with the local flow direction, the stem attaching at least 100 mm downstream of the measurement volume.

## Experimental Results and Discussion

Results are presented by the use of a two-coordinate systems. Blade-row aligned coordinates $(X, Y, Z)$, defined in the axial, spanwise, and pitchwise directions (Fig. 2), are used to reference positions from an origin on the lower endwall at the center of the leading-edge plane of the cascade. The streamline aligned coordinate system $(x_1, x_2, x_3)$, and corresponding mean and fluctuating velocity components $(U_1, U_2, U_3)$ and $(u_1, u_2, u_3)$, are also used in the presentation and analysis of data. In this system, $x_1$ is tangent to the streamlines, whereas $x_3$ is perpendicular to the streamlines in an $X$–$Z$ plane. Most distances are normalized on the axial blade chord $c_a$ of 139 mm, and most velocities on the inlet velocity $U_\infty$ of $24 \pm 1.2$ m/s, corresponding to a Reynolds number (based on the total chord $c$ of 254 mm) of $3.8 \times 10^5 \pm 2 \times 10^4$.

Three-component velocity measurements were made upstream of the central cascade passage at $X/c_a = -0.80$ and $-0.23$; within the passage at $X/c_a = 0, 0.27, 0.48, 0.77$, and 0.98; and downstream at $X/c_a = 1.26$ (Fig. 2). Single-point measurements were made in cross-sectional grids of about 200 points extending pitchwise across the passage (or its extension) and spanwise from the endwall to the midspan of the blades at $Y/c_a = 0.92$. At each point, 50 records of 1024 samples were recorded at a rate of 51.2 kHz and processed to yield mean velocities, Reynolds stresses, and spectra with a low-frequency limit of 50 Hz. These data reveal much about the structure of the flow near the endwall where the endwall boundary layer and tip-leakage vortex dominate. (See Ref. 37 for results and discussion.) They also reveal a closely two-dimensional region at all stations begining at or below $Y/c_a = 0.55$ and extending up through the midspan station. It is this two-dimensional region that is the focus of the present paper.

Two point measurements were also made in this region with the fixed probe placed at selected locations in the midspan plane and the moving probe traversed spanwise from it (in the negative $Y$ direction). The fixed probe locations, shown in Fig. 2, lie along two streamlines obtained by integration of the mean-velocity measurements (shown later), one passing through the center of the passage and the other along its pressure side. Measurements were made for 19 exponentially distributed probe separations at each location. The minimum separation was 3.8 mm ($0.027c_a$). At each separation, 100 records of 4096 samples were recorded simultaneously from both probes at a sampling rate of 51.2 kHz, and processed to yield all nine components of the two-point spanwise space–time correlation and estimates of single- and two-point spectra with a low-frequency limit of 12.5 Hz. Uncertainties of measured quantities calculated at 20:1 odds are given in Table 1.

### Turbulent Inflow

The turbulent inflow generated by the grid is shown in Fig. 3, in terms of pitchwise $(Z)$ profiles of the Reynolds stress components

**Table 1 Uncertainty estimates**

| Quantity | Uncertainty (20:1 odds) |
|---|---|
| $U_i$ | $\pm 1\% U_\infty$ |
| $\overline{u_1^2}$ | $\pm 4\% \overline{u_1^2}$ |
| $\overline{u_2^2}$, $\overline{u_3^2}$ | $\pm 8\% \overline{u_2^2}$, $\overline{u_3^2}$ |
| $\overline{u_i u_j}$ | $\pm 3\% \sqrt{\overline{u_i^2 u_j^2}}$ |
| $k$ | $\pm 3.5\% k$ |

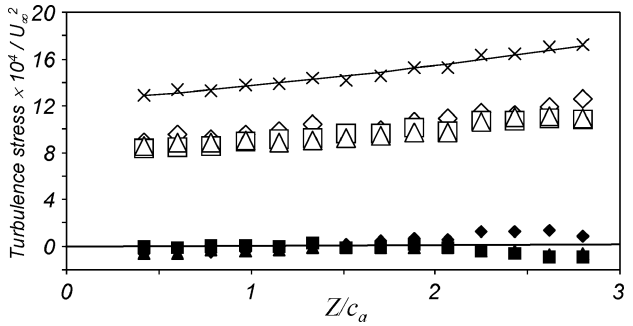


**Fig. 3 Pitchwise turbulence distribution at $X/c_a = -0.80$: ◇, $\overline{u_1^2}$; □, $\overline{u_2^2}$; △, $u_3^2$; ■, $\overline{u_1 u_2}$; ▲, $\overline{u_2 u_3}$; ◆, $\overline{u_1 u_3}$; and ×, $k$; ——, curve fit of Eq. (1); all quantities multiplied by $10^4$ and normalized on $U_\infty^2$.**

and turbulence kinetic energy at $X/c_a = -0.80$. The mean flow here is essentially uniform and equal to the inflow velocity $U_\infty$. Like all single-point measurements presented in this paper, these data have been spanwise averaged (to minimize uncertainties) over the measured portion in the two-dimensional region, that is, from $Y/c_a = 0.55$ to 0.92. Note that the center-passage streamline shown in Fig. 2 crosses this inflow plane at $Z/c_a = 1.69$.

These measurements show the inflow turbulence to have a near-isotropic Reynolds stress tensor, even though the grid was not situated in the contraction,[44] and the turbulence was subjected to an 8% diffusion over the porous bleed slot. The shear stresses are all zero to within their uncertainty, and the normal stresses are almost equal. Averaging in $Z$ shows the cross stream turbulence intensities $\sqrt{u_2^2}$ and $\sqrt{u_3^2}$ to be on average 3.6% less than the streamwise turbulence intensity $\sqrt{u_1^2}$, which compares to the 10% anisotropy normally expected in grid-generated turbulence. Closest to the center streamline, the streamwise turbulence intensity was recorded as 3.1%, which we define as the freestream turbulence level, $\sqrt{u_\infty^2}/U_\infty$.

Because of the 65.1 deg between the cascade and grid, different points in the inflow plane are at different distances downstream of the grid. The resulting gradient in turbulence stresses and kinetic energy across the inflow plane is clearly visible in Fig. 3. Although this gradient had no measurable effect on the mean periodicity of flow through the cascade,[36,37] it does allow those parameters controlling the streamwise evolution of the grid turbulence to be estimated from the pitchwise inflow data. A least-squares linear fit to the turbulence kinetic energy profile of Fig. 3 gives a slope $\partial k/\partial Z = 1.82 \times 10^{-4} U_\infty^2/c_a$. Division by the cosine of the 24.9 deg between the pitchwise $Z$ direction and the flow direction $x_1$ at this station gives the gradient of turbulence kinetic energy along the flow direction, and, thus, with Taylor's hypothesis, the dissipation rate $\varepsilon_\infty = \mathrm{D}k/\mathrm{D}t = U_\infty \partial k/\partial x_1 = 2.0 \times 10^{-4} U_\infty^3/c_a$. Including similar freestream turbulence kinetic energy measurements made at $X/c_a = -0.23$ (providing a somewhat longer range view) in a least-squares fit, we find that the evolution of freestream turbulence levels approaching the cascade is quite accurately described by the relation,

$$k\big/U_\infty^2 = (891 + 116 t U_\infty/c_a)^{-1} \tag{1}$$

where $t$ is the convection time of the turbulence from a line perpendicular to the freestream that passes through the origin of the $X$, $Z$ coordinate system. Upstream of the cascade, $t$ is approximated as $[X \cos(65.1 \text{ deg}) - Z \sin(65.1 \text{ deg})]/U_\infty$. The use of a slightly higher exponent (around 1.3) might be more consistent with earlier grid turbulence studies[45] but makes no significant difference ($<2.5\%k$) to the resulting curve or its extrapolation over the measured length of this flow.

Measurements of the two-point spanwise space–time correlation of the inflow turbulence are shown in Fig. 4. The measurements were made in at $X/c_a = -0.80$, $Z/c_a = 1.71$, very close to the center streamline. The correlation coefficient function is defined as

$$R_{ij}(\Delta x_2, \tau; X, Y, Z) = \frac{\overline{u_i(X, Y, Z, t) u_j(X, Y + \Delta x_2, Z, t + \tau)}}{\sqrt{\overline{u_i(X, Y, Z)^2} \overline{u_j(X, Y, Z)^2}}} \tag{2}$$

(no summation implied). The axes of Fig. 4 are normalized by the longitudinal integral length scale inferred from these measurements. Streamwise integral scales may, in general, be calculated by the use of Taylor's hypothesis as

$$L_{ii} = \frac{U_1}{2} \int_{-T/2}^{T/2} R_{ii}(0, \tau)\, \mathrm{d}\tau \tag{3}$$

(no summation implied) where, for brevity, we have dropped the explicit indication if $X$, $Y$, $Z$ dependence and where $T$ is the velocity record length, equal to $0.8s$ for the two–point measurements. These calculations give a longitudinal correlation $L_{11}$ of 26.1 mm and lateral correlations $L_{22}$ and $L_{33}$ that are 46 and 43% of this value, respectively, quite close to the 50% expected of isotropic turbulence.

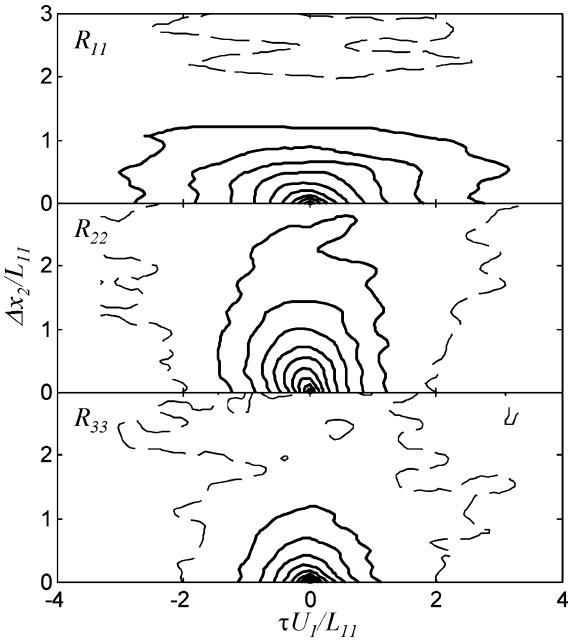


**Fig. 4 Spanwise space–time correlations measured upstream of the cascade at $X/c_a = -0.80$; contours in steps of 0.1; – – –, zero level.**

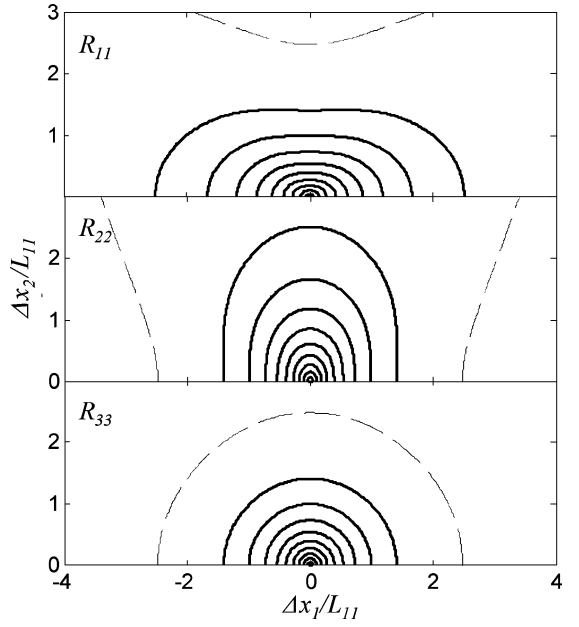


**Fig. 5 Spanwise space–time correlations implied by a von Kármán turbulence spectrum[46]; contours in steps of 0.1; – – –, zero level.**

We define the freestream integral scale ($L_{11\infty}$) as 26.1 mm, this distance being 10% of the blade chord and 26% of the blade spacing projected in the upstream direction. Note that the single-point velocity measurements were used to estimate the pitchwise distribution of streamwise length scales at $X/c_a = -0.80$ (see Ref. 36). Although the record length of the single-point measurements ($0.2s$) was too short to obtain fully resolved integral scale estimates (values were about 85% of the preceding), these measurements indicated no significant variation in the integral length scales upstream of the cascade.

Figure 5 shows, on the same scales as the measurements, the correlation functions implied by the von Kármán interpolation formula for homogeneous turbulence. (See, for example, Hinze.[46]) The comparison shows the form of the measured correlations to be quite closely described by the von Kármán model, particularly in the $R_{11}$ and $R_{22}$ components. The streamwise extent of $R_{22}$ is a little less

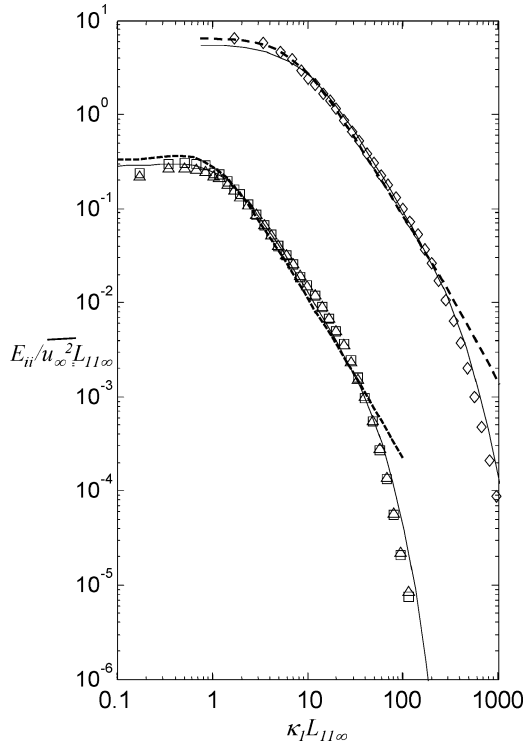


**Fig. 6 Velocity spectra on the center streamline at $X/c_a = -0.80$; ◇, $E_{11}$; □, $E_{22}$; and △, $E_{33}$; ----, von Kármán[46] interpolation and ——, Pope[47] interpolation, evaluated with $L_{11\infty}$ and $\varepsilon_\infty$ ($E_{11}$ spectra and interpolations shifted one decade to right and up).**

than that implied by the model, an imperfection already reflected in the smaller than ideal value of $L_{22}$ just discussed. A similar effect is visible in $R_{33}$ in both the streamwise and spanwise directions.

Turbulence spectra may be obtained by Fourier transformation of these measured correlation functions. In general, the one-dimensional wave number spectrum may be estimated as

$$\frac{E_{ij}(\kappa_1)}{\sqrt{\overline{u_i^2}\overline{u_j^2}}} = \frac{2}{2\pi U_1}\int_{-T/2}^{T/2} R_{ij}(0,\tau)e^{-j\kappa_1 U_1\tau}\,\mathrm{d}\tau \tag{4}$$

(no summation implied), where $\kappa_1$ is the wave number in the flow direction. Plots of $E_{11}$, $E_{22}$, and $E_{33}$ are compared in Fig. 6 with the von Kármán and Pope[45] spectral models. These model forms are most easily written for the three-dimensional wave number spectrum:

$$\Phi_{ij}(\kappa_1,\kappa_2,\kappa_3) = [E(\kappa)/4\pi\kappa^2]\left(\delta_{ij} - \kappa_i\kappa_j/\kappa^2\right) \tag{5}$$

where $\kappa$ is wave number magnitude and $E_{ij}(\kappa_1)$ the integral of $\Phi_{ij}$ with respect to $\kappa_2$ and $\kappa_3$. (See, for example, Pope.[45]) The von Kármán interpolation function for the energy spectrum function $E(\kappa)$ is

$$E(\kappa) = \frac{110kL_{11}}{27\pi C_1^4}\frac{(\kappa L_{11})^4}{\left[1+(\kappa L_{11})^2/C_1^2\right]^{17/6}} \quad \text{where} \quad C_1 = \frac{\sqrt{\pi}\,\Gamma\left(\frac{5}{6}\right)}{\Gamma\left(\frac{1}{3}\right)} \tag{6}$$

The Pope function, expressed in the same terms, that is, $L_{11}$ and $k$, is

$$E(\kappa) = 2CL_{11}k(2\kappa L_{11})^{\frac{5}{3}}\left[\frac{\kappa L_{11}}{\sqrt{(kL_{11})^2+4c_L}}\right]^{\frac{5}{3}+p_o} \times \exp\left(-\beta\left[\sqrt[4]{(\kappa\eta)^4+c_\eta^4}-c_\eta\right]\right) \tag{7}$$

where $C = 1.5$, $p_o = 2$, $c_L = 6.78$, $c_\eta = 0.40$, and $\eta$ is the Kolmogorov microscale $(\nu^3/\varepsilon)^{1/4}$. Figure 6 includes the one-dimensional spectral curves implied by both functions evaluated with $L_{11\infty}$ and $\varepsilon_\infty$.

Figure 6 shows that all three components of the measured spectra are quite closely consistent with both von Kármán and Pope forms at low wave numbers and in the inertial subrange, which is seen to extend over about one and one-half decades. At higher wave numbers, the von Kármán interpolation makes no allowance for dissipation. Pope's interpolation does, however, and there is some agreement between the shape of these curves and the experimental data in this range. The experimental spectra fall off somewhat faster than Pope's model, however. Although this could be a limitation of the model, it is as likely due to the finite measurement volume size. A disturbance with a wavelength equal to the measurement volume diameter would have a nondimensional wave number $\kappa_1 L_{11} = 160$, comparable to the wave number range of the roll off.

### Flow Through the Cascade

The mean flowfield through the cascade between $X/c_a = -0.23$ and 1.26 is shown in Figs. 7 and 8 in terms of contours of mean velocity magnitude $U_1/U_\infty$ and mean velocity vectors. Note that the vectors are drawn at the actual midspan measurement locations.

These plots reveal the mean velocity field that convects and distorts the incident turbulence passing through the central passage. Flow passing near the suction side of the passage experiences an acceleration of a few percent over the first half of blade 4, followed by a much steeper deceleration to the cascade exit velocity of close to $71\%U_\infty$. On the pressure side of the passage, this deceleration occurs over the first half chord of blade 5 with the result that many of the mean velocity contours cross the passage almost perpendicular to the local flow direction. That direction, of course, changes in the cascade, as evidenced by the mean velocity vectors, the measured exit angle being 11.8 deg from the inlet angle near midpassage. Both vectors and contours show evidence of the viscous boundary layers formed on the blade surfaces, particularly at the more downstream stations. The only significant thickening of the boundary layers occurs on the suction side of the trailing edge of blade 4, possibly indicating a small region of separation here.

Included for comparison in Figs. 7 and 8 are results from the Reynolds-averaged Navier–Stokes (RANS) solution of Shin.[47] He

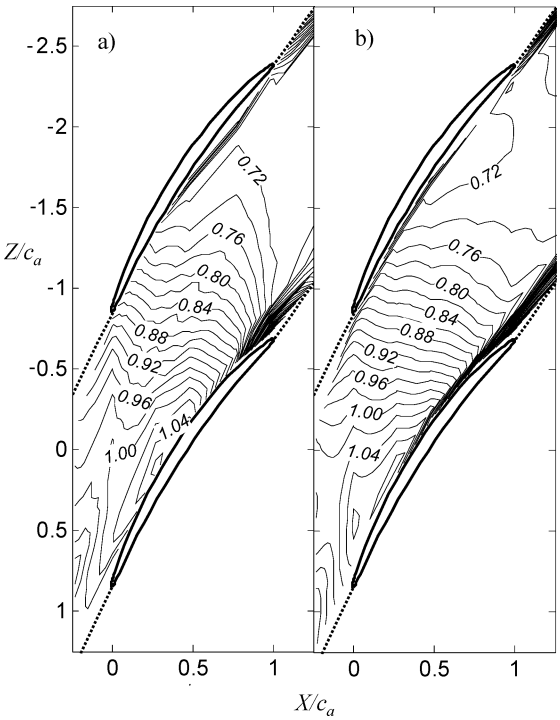


**Fig. 7 Contours of mean velocity magnitude $U_1/U_\infty$: a) measured and b) computed.[47]**

reports two-dimensional RANS calculations for the present cascade geometry and inflow conditions (but without grid turbulence) using an unstructured grid and Spallart–Almaras turbulence model. Shin[47] describes fairly extensive tests to validate the code and establish convergence. There are some points of disagreement between the experimental results and those of the RANS solution. The acceleration over the suction side of blade 4 produces velocities some 2% greater than those measured, and the details of the shapes of the measured velocity contours in the downstream half of the passage are not accurately reproduced in the RANS. Otherwise, however, measurement and computation appear in close agreement, both in terms of global parameters such as outlet velocity and direction ($0.708U_\infty$ and 11.7 deg in the RANS results) and in many of the smaller flow details, such as the extent of the viscous regions and the kinks in the velocity contours near the cascade leading-edge line. This agreement provides some independent verification of the experimental results, of the two dimensionality of the measured flow near the cascade midspan, and of the proper operation of the cascade.

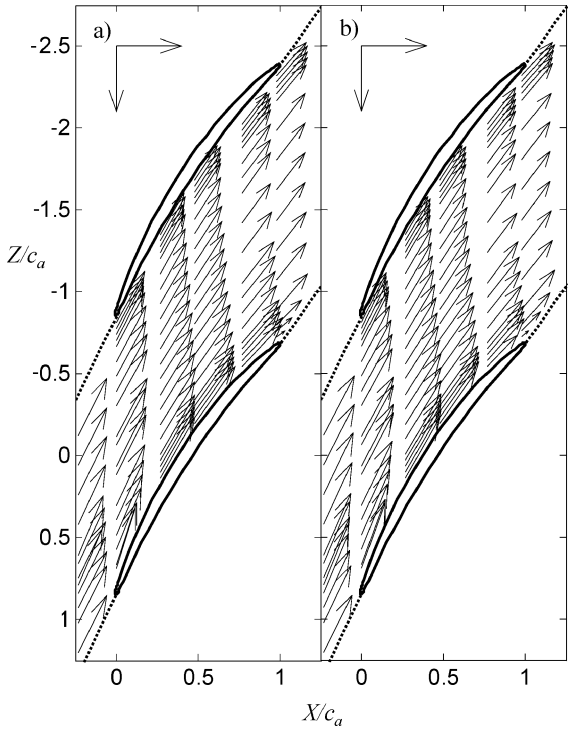


**Fig. 8 Mean velocity vectors: ↓→, are of length $U_\infty$: a) measured and b) computed.[47]**

Figure 9 shows contours of the three Reynolds normal stresses in the blade passage. These distributions are perhaps most remarkable for what they do not show. Based on the rate of decay of the turbulence measured at the inflow [Eq. (1)], one would expect about a 25% reduction in the normal stresses over the length of flow represented in the Figs. 9. Outside the thin viscous regions adjacent to the blade surfaces, the streamwise turbulence normal stress $u_1^2$ is almost constant at around $0.0008U_\infty^2$. Consequently, the contour positions are quite uncertain. The spanwise normal stress $u_2^2$ behaves similarly, except near the cascade exit where it falls slightly. The only substantial variations are seen in $u_3^2$, this being the in-plane component perpendicular to the mean flow direction. Near the center of the passage, $u_3^2$ drops by about 40% as the flow passes through the cascade. Levels of this stress are further suppressed over a region that extends about $0.2c_a$ from the blade surfaces, possibly because of the blocking effects of those surfaces. The suppression appears slightly greater on the suction side of the passage.

For the purpose of further analysis and discussion, we focus on two regions visible in the $u_3^2$ distribution, the midpassage region where the influence of the blades is felt only indirectly through the changes in flow direction and velocity they produce and the region adjacent to the pressure side of the passage where the direct effect of the blades, through surface blocking, is likely to dominate.

#### Midpassage Region

Batchelor and Proudman[4] showed that homogeneous distortion of homogeneous turbulence reduces turbulence levels in directions along which the fluid elements are stretched and increases them in directions along which the fluid elements are compressed. The observed drop of $u_3^2$ and increase (compared to its expected decay)

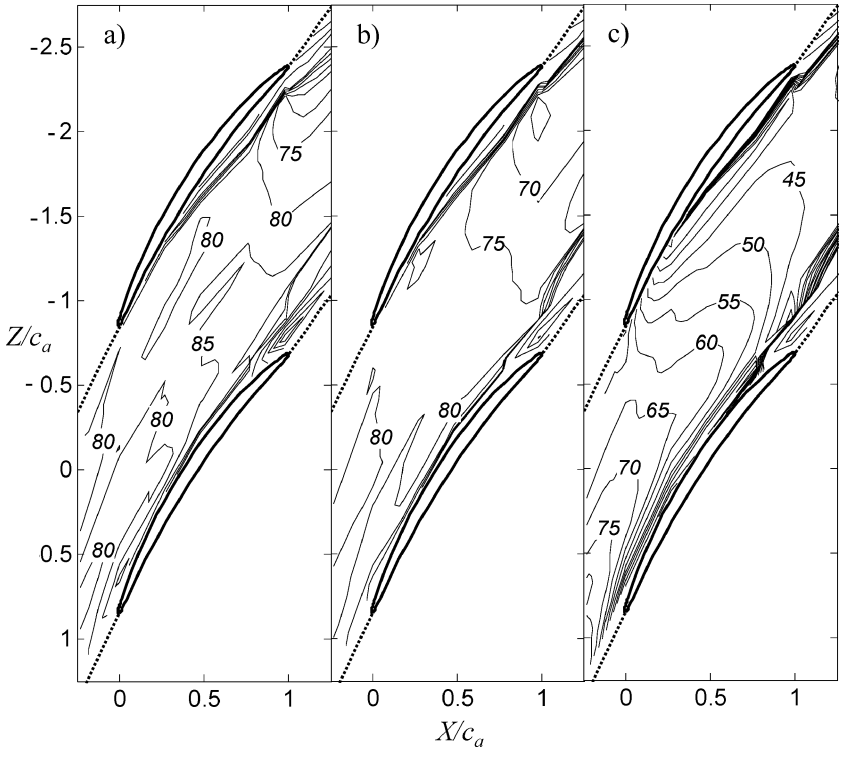


**Fig. 9 Contours of measured turbulence normal stresses: a) $\overline{u_1^2}/U_\infty^2 \times 10^5$, b) $\overline{u_2^2}/U_\infty^2 \times 10^5$, and c) $\overline{u_3^2}/U_\infty^2 \times 10^5$.**

of $\overline{u_1^2}$ in the midpassage region appear qualitatively consistent with these effects superimposed over a background of viscous decay. The important issues here are whether these superimposed variations are quantitatively consistent with RDT and whether such predictive ability would extend to more detailed turbulence information such as velocity spectra.

To address this issue we have performed calculations of the midpassage flow using Goldstein's[48] method. This method accounts for the transport of turbulent vorticity by the mean flowfield but does not model surface blocking effects. It is a high-frequency approximation to RDT that applies to inhomogeneous flows when the distortion produced by the mean flow occurs on a scale that is large compared to that of the turbulence. This is the case near midpassage where distortion occurs on a scale of the order of the blade chord, which is an order of magnitude greater than the turbulence scale $L_{11\infty}$.

In the case of incompressible flow, Goldstein's equation for the wave number spectrum of turbulence $\Phi_{ij}(\kappa_1, \kappa_2, \kappa_3)$, suffering a mean flow distortion, reduces to a form originally derived by Batchelor and Proudman[4]:

$$\Phi'_{ij}(\chi_1, \chi_2, \chi_3) = \varepsilon_{ikl}\varepsilon_{mnp}\varepsilon_{jab}\varepsilon_{uvw}\chi_l\chi_b\chi^{-4}\kappa_n\kappa_v S_{km}S_{au}\Phi_{pw}(\kappa_1, \kappa_2, \kappa_3) \qquad (8)$$

Here, $\Phi_{ij}(\kappa_1, \kappa_2, \kappa_3)$ and $\kappa_i$ are the wave number spectrum and components before the distortion and $\Phi'_{ij}(\chi_1, \chi_2, \chi_3)$ and $\chi_i$ are the spectrum and components distortion. Note that $\kappa_i = \chi_j S_{ji}$. The symbol $\chi$ is used to represent the magnitude of the wave number vector after distortion. The distortion tensor $S_{ij}$ is defined as

$$S_{ij} \equiv \frac{\partial x_i}{\partial a_j} \qquad (9)$$

where $x_i$ represents the mean-flow aligned coordinates already defined, and $a_j$ are the Lagrangian coordinates of the fluid material, defined as equal to $x_i$ in the undistorted free stream ahead of the cascade (Fig. 2). To the degree that the flow is two-dimensional, the cascade produces no distortion in the $x_2$ direction, and so

$$\frac{\partial x_2}{\partial a_2} = 1, \qquad \frac{\partial x_2}{\partial a_1}, \frac{\partial x_2}{\partial a_3}, \frac{\partial x_1}{\partial a_2}, \frac{\partial x_3}{\partial a_2} = 0 \qquad (10)$$

Because $a_1$ and $x_1$ both lie along a mean streamline, $\partial x_1/\partial a_1$ represents the total extension of a streamwise fluid line between the freestream and the midpassage flow, which is simply given by the relative mean velocity magnitude $U_1/U_\infty$. Because both $a_3$ and $x_3$ are perpendicular to the streamlines, $\partial x_3/\partial a_3$ represents the change in mean streamline spacing, which is equal to $U_\infty/U_1$. Of the remaining derivatives, $\partial x_3/\partial a_1$ is zero because the fluid line defined by $a_1$ always remains along a streamline, and $\partial x_1/\partial a_3$ represents the tilting of the fluid line defined by $a_3$ relative to the streamline perpendicular (Fig. 2). As shown in the Appendix, this term can be calculated as a line integral:

$$\frac{\partial x_1}{\partial a_3} = -\frac{U_1}{U_\infty}\int_{\text{streamline}} \frac{\partial\left(U_\infty^2/U_1^2\right)}{\partial x_3}\,\mathrm{d}x_1 \qquad (11)$$

where the integration begins in the freestream and ends at the point where the distortion is desired. Thus, in summary,

$$S_{ij} = \begin{pmatrix} \dfrac{U_1}{U_\infty} & 0 & -\dfrac{U_1}{U_\infty}\displaystyle\int_S \frac{\partial\left(U_\infty^2/U_1^2\right)}{\partial x_3}\,\mathrm{d}x_1 \\ 0 & 1 & 0 \\ 0 & 0 & \dfrac{U_\infty}{U_1} \end{pmatrix} \qquad (12)$$

The measured mean velocity field was interpolated by the use of cubic splines, numerically differentiated (using central differences) and integrated (using the predictor corrector method) to obtain $S_{ij}$ and the streamline paths. This calculation was validated by its repetition with the much smoother, more finely detailed, mean velocity field provided by Shin's[47] CFD solution, which produced very similar results. (Differences were no larger than those that would be expected from the comparison of the mean velocity fields in Figs. 7 and 8.) The undistorted spectrum tensor was specified based on measured turbulence inflow data, that is, using Eqs. (5) and (7) with the longitudinal integral scale $L_{11}$ set to its freestream value of $0.26c_a$. The turbulence kinetic energy required in Eq. (7), however, was not taken as the freestream value but calculated by the use of the measured decay profile expressed in Eq. (1). Thus, the RDT calculations were performed relative to the background of viscous decay inferred from the variation of freestream turbulence levels. Distorted wave number spectra, calculated with Eq. (8), were then integrated over a $64^3$ grid of exponentially spaced wave numbers from $\kappa L_{11\infty} = -300$ to 300 to yield the single-point turbulence statistics, integral scales, and the one-dimensional turbulence spectra throughout the midpassage region. Results were found to be unaltered by an increase in the range or resolution of the wave number grid.

Turbulence stresses in the cascade calculated using this method are shown in Fig. 10. Overall, the RDT method appears to predict quite well the arrested decay that characterizes the streamwise ($\underline{u_1^2}$) and spanwise ($\underline{u_2^2}$) normal stresses near midpassage. The predicted stresses are about $0.00005U_\infty^2$ less than those measured (6–7%), but this difference appears to be almost constant, which suggests that it may be associated with implicit differences in the initial condition. Indeed, this difference may partly result from the slight anisotropy of the incident turbulence normal stresses that was not modeled in the RDT calculation.

The calculations also reproduce the rapid drop in the $\overline{u_3^2}$ stress experienced in the midpassage region. The accuracy of the calculations in this region is similar to that seen in the other components, but the difference (seen in the upstream half of the passage) is in the opposite direction; at most stations, predicted values of $\underline{u_3^2}$ lie about $5 \times 10^{-5}U_\infty^2$ above those measured.

Measured and calculated one-dimensional velocity spectra at various locations along the passage center streamline are compared in Fig. 11. These plots show how the spectral distribution of energy making up the normal stresses varies through the cascade, and the extent to which that variation is consistent with the RDT model. The measured streamwise fluctuation spectra $E_{11}$ show only a slight reduction in level and no significant change in shape through the cascade. $E_{22}$ are similarly invariant, except for a small reduction in spectral levels at low frequencies as the flow enters the cascade. By far the largest changes occur in the $E_{33}$ component. As the flow passes through the cascade, spectral levels fall significantly. The drop is greatest at low frequencies (about a factor of three) and becomes smaller as the frequency is increased. As a result, there is a noticeable reduction in the slope of the inertial subrange, from 1.45 at the passage entrance to 1.3 at its exit.

Note that the RDT calculated spectra display almost the same behavior. The lack of variation in the predicted $E_{11}$ spectrum and the bulk of the $E_{22}$ spectrum is consistent with the experimental results and adds weight to the conclusion that it is rapid-distortion effects that arrest the decay of these components in the passage. The $E_{33}$ spectrum provides a more explicit test of the predictive capability of the theory. We see here that, except at the very highest frequencies, the predicted spectra closely follow those measured, matching not only the reduction in spectral levels at low frequencies but also the fall in slope of the inertial subrange.

**Pressure-Side Region**

We define the pressure-side region as within 1–1.5 freestream integral scales ($L_{11\infty} = 0.26c_a$) of the pressure-side blade. In this region, one would expect the turbulence to be modified additionally by the blocking of normal velocity fluctuations at the blade surface. Indeed, the suppression of normal velocity fluctuations close to the blade in Fig. 9c strongly suggests the presence of such effects. What is important here, of course, is whether the details of these effects (and thus, by implication, the physics behind them) are quantitatively consistent with the linearized blade-blocking effects that are modeled by RDT. We choose to focus on the pressure side

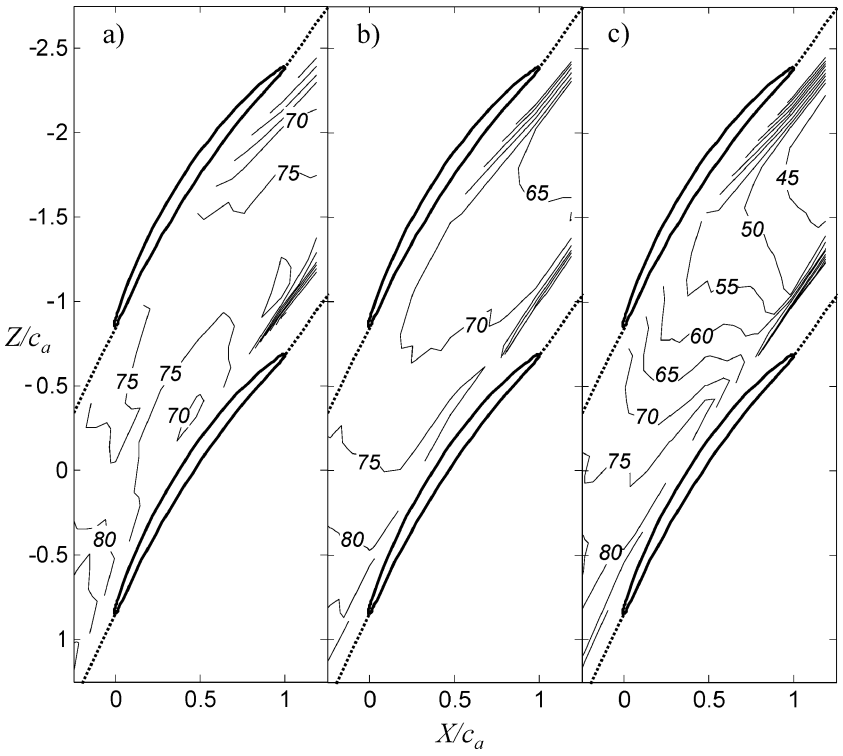


**Fig. 10 Contours of turbulence normal stresses computed with RDT: a) $\overline{u_1^2}/U_\infty^2 \times 10^5$, b) $\overline{u_2^2}/U_\infty^2 \times 10^5$, and c) $\overline{u_3^2}/U_\infty^2 \times 10^5$.**

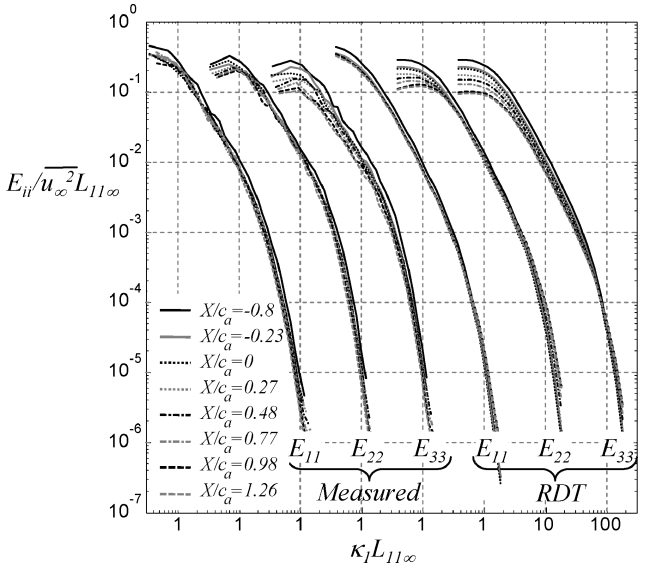


**Fig. 11 Autospectra of velocity fluctuations along the center streamline shown in Fig. 2.**

(as opposed to the suction side) because more detailed measurements were available here, the pressure side being more accessible to probes mounted from downstream.

A complete RDT calculation of the surface blocking produced by the full cascade geometry would be a substantial undertaking, well beyond the scope of the present work. Instead we have employed Hunt and Graham's[16] theory to provide approximate predictions of stress variations, velocity spectra, and two-point correlations for comparison with the measurements. This approach, of course, treats the pressure-side cascade blade as though it were a flat plate in an infinite stream. This may be justifiable given the thinness and only gradual camber of the blade, its sharp leading edge at near zero angle of attack, and the small size of the incident turbulence scale compared to the blade spacing. However, it means that predictions will not account for changes to the turbulence resulting from mean flow distortion through the cascade, or viscous decay, changes that we will incorporate approximately by normalization on local turbulence levels.

For the case of the surface blocking of a homogeneous turbulent flow in the $x_1$ direction encountering a flat plate, perpendicular to $x_3$, Hunt and Graham[16] give an explicit expression for the two-point one-dimensional wave number spectrum:

$$E_{ij}(\boldsymbol{x}, \boldsymbol{x}', \kappa_1) = \int_{-\infty}^{\infty}\int_{-\infty}^{\infty} M_{il}^*(x_1, x_3, \boldsymbol{\kappa}) M_{jm}(x_1', x_3', \boldsymbol{\kappa}) \times \exp[i\kappa_3(x_2 - x_2')]\Phi_{lm}(\boldsymbol{\kappa})\, \mathrm{d}\kappa_2\, \mathrm{d}\kappa_3 \quad (13)$$

where $\boldsymbol{x}$ and $\boldsymbol{x}'$ are the position vectors $(x_1, x_2, x_3)$ of the two points, $\boldsymbol{\kappa}$ is the wave number vector $(\kappa_1, \kappa_2, \kappa_3)$, $x_3$ is measured from the surface, and

$$M_{ij}(x_1, x_3, \boldsymbol{\kappa}) = \delta_{ij} \exp[i(\kappa_1 x_1 + \kappa_3 x_3)] + \delta_{j3} \exp\left(i\kappa_1 x_1 - x_3\sqrt{\kappa_1^2 + \kappa_2^2}\right)\left(\frac{\delta_{i1} i\kappa_1 + \delta_{i2} i\kappa_2}{\sqrt{\kappa_1^2 + \kappa_2^2}} - \delta_{i3}\right) \quad (14)$$

Hunt and Graham[16] intended for these equations to apply for distances from the leading edge $x_1 - x_1|_{\mathrm{le}} \geq L_{11\infty}$ and $x_1 - x_1|_{\mathrm{le}} \ll L_L$, where $L_L$ is the eddy turnover distance. Equation (13) was evaluated with the same $64^3$ logarithmically spaced wave number grid used earlier, the results again being range and resolution independent. The undistorted spectrum tensor $\Phi_{ij}$ was specified based on measured turbulence inflow data, that is, by the use of Eqs. (5) and (7), with the longitudinal integral scale given its measured freestream value $L_{11\infty} = 0.26c_a$.. The resulting two-point one-dimensional spectral estimates were then integrated or Fourier transformed as appropriate to yield turbulent stresses and two-point correlations.

Turbulence normal stress profiles ($\overline{u_1^2}$ and $\overline{u_3^2}$) measured close to the blade surface on the pressure side of the passage are compared with Hunt and Graham's[16] solution in Fig. 12. Profiles were measured in the pitchwise direction but are shown here as a function of perpendicular distance from the blade surface $x_3$. One-dimensional

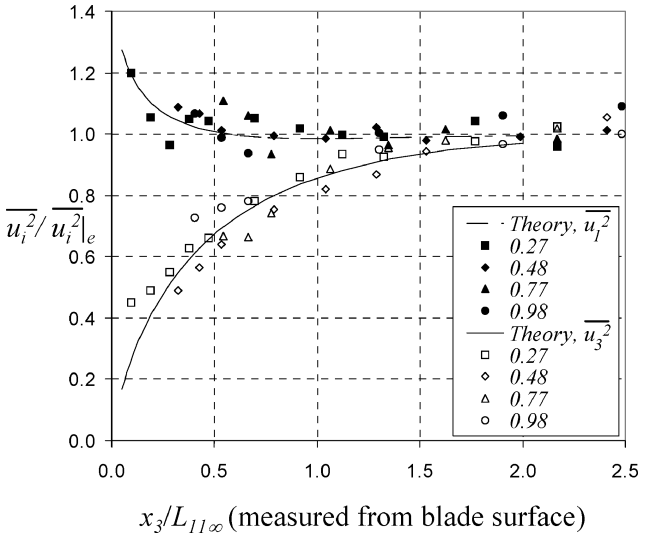


**Fig. 12 Turbulence stress profiles in the pressure-side region adjacent to blade 5, plotted as a function of perpendicular distance from the blade and compared with Hunt and Graham's[16] solution; numbers in legend indicate $X/c_a$ location.**

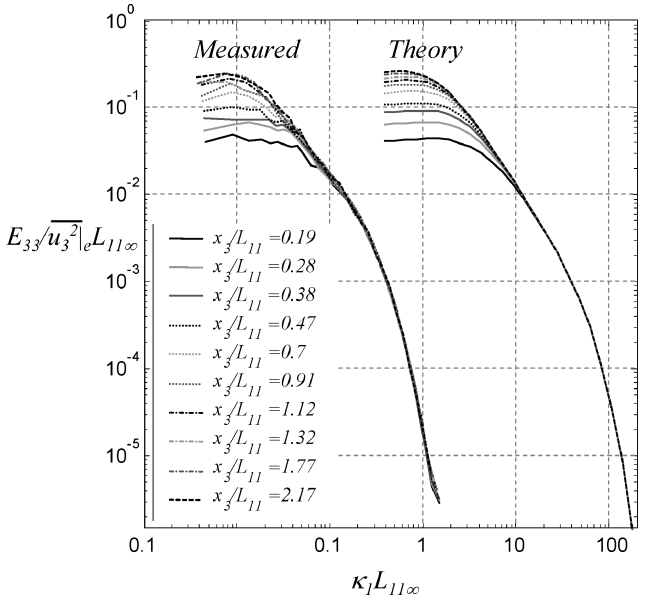


**Fig. 13 Autospectra of velocity fluctuations at $X/c_a = 0.27$ in the pressure-side region adjacent to blade 5, plotted as a function of perpendicular distance from the blade and compared with Hunt and Graham's[16] solution.**

spectra of normal-to-surface velocity fluctuations $E_{33}$, measured as part of the same profiles, are also compared with theory in Figs. 13 and 14. Measured stresses and spectra have been normalized on midpassage stress levels at the same axial station $\overline{u_i^2}|_e$. Measurements obviously in the viscous boundary layer (characterized by much higher stress and high-frequency spectral levels) have been eliminated from Figs. 13 and 14.

The measured stress profiles show in detail the stress variations close to the pressure-side blade. They reveal that the proximity of the blade surface has almost no effect on the intensity of streamwise velocity fluctuations $\overline{u_1^2}$. They also show the extent and form of the suppression of the turbulence stress normal to the blade $\overline{u_3^2}$, which falls to near half of its midpassage value closest to the blade surface. In the normalized form of Fig. 12, both sets of profiles appear approximately invariant with streamwise position. To within their scatter, they are described well by the curves computed from Hunt and Graham's[16] theory.

The spectra reveal how the suppression of velocity fluctuations normal to the blade surface is broken down by frequency and, thus,

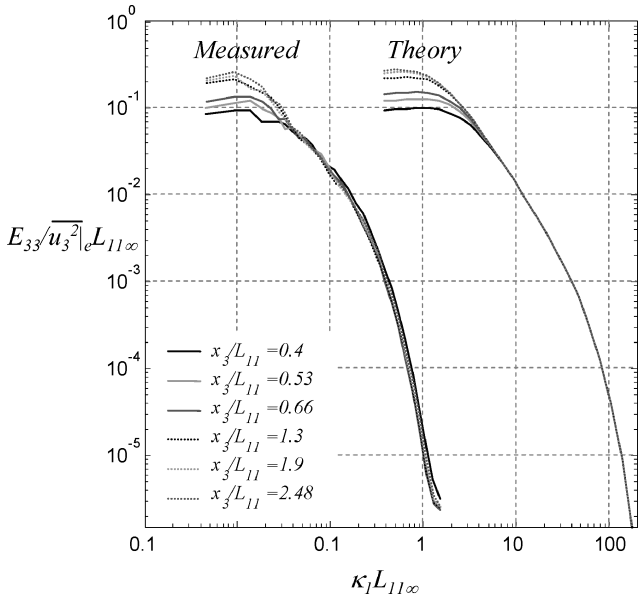


**Fig. 14 Autospectra of velocity fluctuations at $X/c_a = 0.98$ in the pressure-side region adjacent to blade 5, plotted as a function of perpendicular distance from the blade and compared with Hunt and Graham's[16] solution.**

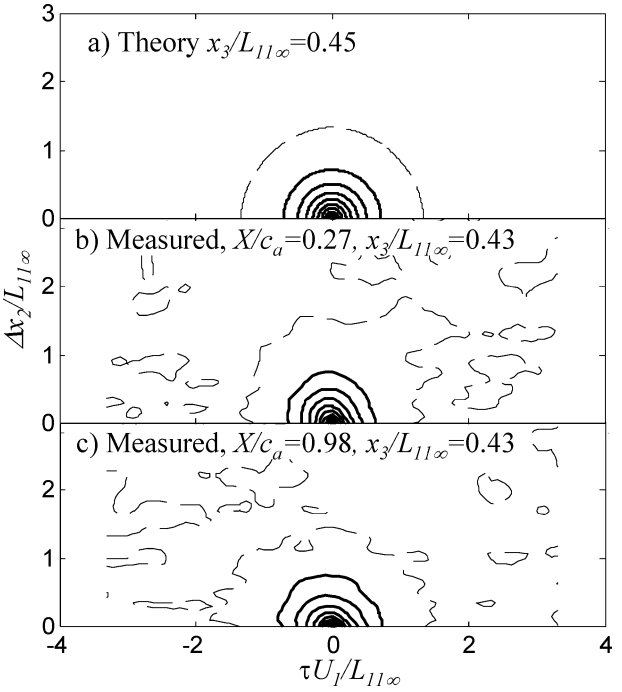


**Fig. 15 Spanwise space–time correlations in the pressure-side region adjacent to blade 5 compared with Hunt and Graham's[16] solution: contours in steps of 0.1; – – –, zero level.**

scale. The measurements at both stations clearly show that it is the low-frequency, large-scale fluctuations that are attenuated near the surface and that the degree of attenuation, and upper limit of frequencies affected, increases as the surface is approached. High-frequency turbulent fluctuations are almost completely unaffected. This behavior appears to be in convincing agreement with Hunt and Graham's[16] theory. The shapes of the theoretical spectra, the range and magnitude of the suppression they show, and the variation of that suppression with distance from the surface, all closely track the measured data. Note that the correlation between measurement and theory appears almost as good at the blade trailing edge, some 10 integral scales downstream of the leading edge, as it does at the quarter chord.

This agreement suggests that, despite its approximate nature and the compromises made in its comparison with experiment, this theory somehow captures the dominant physics controlling the behavior of the turbulence close to the blade. This idea is reinforced by the behavior of the spanwise two-point correlations. Correlations of $u_3$ velocity fluctuations measured about half of an integral scale from the blade surface at $X/c_a = 0.27$ and 0.98 are compared with theory in Fig. 15. A two-dimensional comparison is made by equating time delay between the two probes in the experiment, $\tau$ to streamwise separation, by the use of Taylor's hypthesis, that is $x_1 - x_1' = -\tau U_1$. Correlations of $u_2$ and $u_1$ were also measured but are not shown here because, in agreement with the theory, they are not significantly different than the freestream correlations shown in Fig. 4. The $u_3$ correlation, however, is substantially affected. Hunt and Graham's[16] theory (Fig. 15a) predicts that the proximity of the surface should reduce the extent of the $u_3$ correlation function by about one-half compared to its freestream form, this contraction being isotropic in the streamwise and spanwise directions. The measurements (Figs. 15b and 15c) show almost exactly this effect, even to the extent that the measured correlation functions are slightly more compact than the prediction, just as the measured freestream $u_3$ correlation function (Fig. 4) is slightly more compact than the model function provided to the theory as input. As with the spectra, the RDT model appears just as accurate at the trailing edge as at the one-quarter chord.

## Conclusions

The behavior of turbulence flowing through a compressor cascade has been measured and compared with predictions using RDT. The cascade, operated at a chord Reynolds number of $3.8 \times 10^5$, produces a turning of 11.8 deg. Turbulence was generated with a biplanar grid positioned across the flow some 20 grid-cell sizes upstream of the cascade. Measurements were made in the two-dimensional region near the midspan of the cascade by the use of single- and two-point three-component hot-wire anemometry.

The freestream turbulence approaching the cascade has a near-isotropic Reynolds stress tensor and a turbulence intensity of 3.1%. The longitudinal integral scale ($L_{11\infty}$) is 26.1 mm, equivalent to 26% of the blade spacing projected in the upstream direction. Lateral correlation length scales and spanwise two-point space–time correlations are consistent with the expectations of homogeneous isotropic turbulence. Velocity spectra fit closely to Pope's[45] interpolation formula when evaluated with the measured turbulence intensity, length scale, and dissipation rate.

The decay of this turbulence (which follows an inverse relationship with streamwise distance upstream of the cascade), is substantially modified by the deceleration and turning of the flow in the cascade. Near the passage center, the decay of the streamwise and spanwise turbulence normal stresses $u_1^2$ and $u_2^2$ is almost completely halted, the outlet values of these stresses being nearly as large as those at the inlet. Conversely, the drop in $u_3^2$ is accelerated, this stress falling by about 40% to the cascade exit. Calculations performed with Goldstein's[48] method show these variations to be quantitatively consistent with these RDT effects superimposed over a background of viscous decay. The quantitative realism of the RDT results extends to the velocity spectra. On the passage center streamline, streamwise velocity autospectra $E_{11}$ are almost invariant, spanwise spectra $E_{22}$ show small reductions in low-frequency levels, and $E_{33}$ spectra show large reductions at low frequencies and an associated change in the slope of the inertial subrange, effects all predicted by the theory.

Near the blades, the turbulence is additionally modified by the blocking of normal ($u_3$) velocity fluctuations. Profiles measured close to the pressure-side blade show the extent and form of the suppression in terms of the $u_3^2$ turbulence stress that falls to near one-half of its center passage value, close to the blade surface. Normalized on these values, stress profiles measured in this region are almost invariant with streamwise position and in agreement with Hunt and Graham's[16] RDT theory for surface blocking produced by a flat plate. Although this theory does not account for changes to the turbulence resulting from mean flow distortion through the cascade, it also provides accurate predictions of $u_3$ spectra. Specifically, the shapes of the theoretical spectra, the range and magnitude of the suppression they show, and the variation of that suppression with distance from the surface all closely track the measured data. The theory also accurately predicts the contraction of the spanwise space–time correlation function in the vicinity of the blade surface. Note that the agreements between measurement and theory appear almost as good at the blade trailing edge as at the quarter chord.

Overall, we find that the measured evolution of turbulence through the cascade, including its spectrum and space–time correlations, is quantitatively consistent with RDT effects superimposed over a background of viscous decay. This suggests that, at least in circumstances similar to those modeled here, RDT-based models offer a viable approach for the calculation of the modification of turbulence passing through a blade row.

## Appendix: Derivation of Equation (11)

Figure A1 shows a streamline connecting a general point in the flow $P$ to a corresponding point in the freestream $O$. We wish to determine the derivative $\partial x_1/\partial a_3$, where the $x_i$ are streamline aligned coordinates at $P$ and the $a_i$ are Lagrangian coordinates representing the initial position of the fluid material at $O$. Consider an element of a fluid line $OO'$, initially perpendicular to the flow direction, that convects to $PP'$ in time $t$. If the initial length of the line is $\delta a_3$, then $(\partial x_1/\partial a_3)\delta a_3$ is the streamwise component of the line length at $t$. If the time taken for the flow to convect from $O'$ to $P''$ is $t$–$\delta t$, where $PP''$ is a streamline normal, then

$$\frac{\partial x_1}{\partial a_3}\delta a_3 = U_1 \delta t \tag{A1}$$

where $U_1$ is the flow velocity. If the stream function of the streamline $OP$ is $\psi$, then that of the streamline $O'P''$ is $\psi + \delta\psi$ where $\delta\psi = U_\infty \delta a_3 = U_1 \delta x_3$. Thus, we may write

$$t = \int_{\text{streamline } OP} \frac{1}{U_1}\,\mathrm{d}x_1 = \int_{\phi_O}^{\phi_P} \left(\frac{1}{U_1^2}\right)_\psi \mathrm{d}\phi \tag{A2}$$

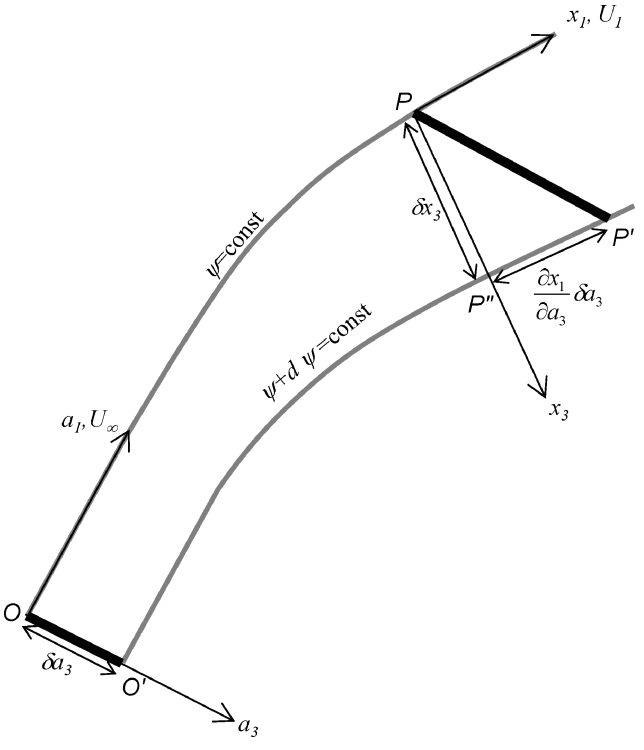


**Fig. A1 Nomenclature for Appendix.**

where $\phi$ is the velocity potential, and

$$t - \delta t = \int_{\phi_{O'}}^{\phi_{P''}} \left(\frac{1}{U_1^2}\right)_{\psi+\delta\psi} \mathrm{d}\phi = \int_{\phi_O}^{\phi_P} \left(\frac{1}{U_1^2}\right)_{\psi+\delta\psi} \mathrm{d}\phi \quad \text{(A3)}$$

where we make use of the fact that $OO'$ and $PP''$ are both equipotentials. Thus,

$$\delta t = \int_{\phi_O}^{\phi_P} \left(\frac{1}{U_1^2}\right)_{\psi} - \left(\frac{1}{U_1^2}\right)_{\psi+\delta\psi} \mathrm{d}\phi = -\delta\psi \int_{\phi_O}^{\phi_P} \frac{\partial\left(1/U_1^2\right)}{\partial\psi} \mathrm{d}\phi$$

$$= -U_\infty \delta a_3 \int_{\text{streamline } OP} \frac{\partial\left(1/U_1^2\right)}{\partial x_3} \mathrm{d}x_1 \quad \text{(A4)}$$

By substitution into Eq. (A1), we obtain

$$\frac{\partial x_1}{\partial a_3} = -\frac{U_1}{U_\infty} \int_{\text{streamline } OP} \frac{\partial\left(U_\infty^2/U_1^2\right)}{\partial x_3} \mathrm{d}x_1 \quad \text{(A5)}$$

## Acknowledgments

The authors thank the U.S. Office of Naval Research, in particular Ronald Joslin and Patrick Purtell, for their support under Grants N00014-99-1-0230 and N00014-03-1-0199. Numerical data from the experiments described here are available from URL: http://www.aoe.vt.edu/flowdata.

## References

[1]Hanson, D. B., and Horan, K., "Turbulence/Cascade Interaction: Spectra of Inflow, Cascade Response and Noise," AIAA Paper 98-2319, 1998.

[2]Glegg, S. A. L., " Prediction of Blade Wake Interaction Noise Based on a Turbulent Vortex Model," *AIAA Journal*, Vol. 29, No. 10, 1991, pp. 1545–1551.

[3]Blake, W. K., *Mechanics of Flow Induced Sound and Vibration*, Academic Press, New York, 1986.

[4]Batchelor, G. K., and Proudman, I., "The Effect or Rapid Distortion on a Fluid in Turbulent Motion," *Quarterly Journal of Mechanics and Applied Mathematics*, Vol. 7, Pt. 1, 1954, pp. 83–103.

[5]Hunt, J. C. R., "A Theory of Turbulent Flow Around Two-Dimensional Bluff Bodies," *Journal of Fluid Mechanics*, Vol. 61, Pt. 4, 1973, pp. 625–706.

[6]Golubev, V. V., and Atassi, H. M., "Acoustic Vorticity Waves in Swirling Flows," *Journal of Sound and Vibration*, Vol. 209, 1998, pp. 203–222.

[7]Atassi, H. M., "Aeroacoustics of Non-Uniform Flows," AIAA Paper 97-0378, Jan. 1997.

[8]Fang, J., and Atassi, H. M., "Numerical Solutions for Unsteady Subsonic Vortical Flows Around Loaded Cascades," *Journal of Turbomachinery*, Vol. 115, No. 4, 1993, pp. 810–816.

[9]Atassi, H. M., Fang, J., and Patrick, S., "Direct Calculation of Sound Radiated from Bodies in Non-Uniform Flows," *Journal of Fluids Engineering*, Vol. 115, 1993, pp. 573–579.

[10]Scott, J. R., and Atassi, H. M., "A Finite-Difference, Frequency Domain Numerical Scheme for the Solution of the Gust Response Problem," *Journal of Computational Physics*, Vol. 119, 1995, pp. 75–93.

[11]Silowski, P. D., and Hall, K. C., "A Coupled Mode Analysis of Unsteady Multistage Flows in Turbomachinery," *Journal of Turbomachinery*, Vol. 120, No. 3, 1998, pp. 410–412.

[12]Lorence, C. B., and Hall, K. C., "Sensitivity Analysis of the Aeroacoustic Response of Turbomachinery Blade Rows," *AIAA Journal*, Vol. 34, No. 8, 1996, pp. 1545–1554.

[13]Peake, N., and Kerschen, E. J., "Influence of Mean Loading on Noise Generated by the Interaction of Gusts with a Flat-Plate Cascade," *Journal of Fluid Mechanics*, Vol. 347, 1997, pp. 315–346.

[14]Majumdar, S. J., and Peake, N., "Noise Generation by the Interaction Between Injested Turbulence and a Rotating Fan," *Journal of Fluid Mechanics*, Vol. 359, 1998, pp. 181–216.

[15]Graham, J. M. R., "The Effect of a Two-Dimensional Cascade of Thin Streamwise Plates on Homogeneous Turbulence," *Journal of Fluid Mechanics*, Vol. 356, 1998, pp. 125–147.

[16]Hunt, J. C. R., and Graham, J. M. R., "Free-Stream Turbulence near Plane Boundaries," *Journal of Fluid Mechanics*, Vol. 84, Pt. 2, 1978, pp. 209–235.

[17]Kullar, I., and Graham, J. M. R., "Acoustic Effects due to Turbulence Passing Through Cascades of Thin Aerofoils," *Journal of Sound and Vibration*, Vol. 110, No. 1, 1986, pp. 143–160.

[18]Uzkan, T., and Reynolds, W. C., "A Shear Free Turbulent Boundary Layer," *Journal of Fluid Mechanics*, Vol. 28, Pt. 4, 1967, pp. 803–821.

[19]Thomas, N. H., and Hancock, P. E., "Grid Turbulence near a Moving Wall," *Journal of Fluid Mechanics*, Vol. 82, Pt. 3, 1977, pp. 481–496.

[20]Perot, B., and Moin, P., "Shear-Free Turbulent Boundary Layers. Part 1. Physical Insights into Near-Wall Turbulence," *Journal of Fluid Mechanics*, Vol. 295, 1995, pp. 199–227.

[21]Walker, D. T., Leighton, R. I., and Garza-Rios, L. O., "Shear Free Turbulence near a Flat Free Surface," *Journal of Fluid Mechanics*, Vol. 320, 1996, pp. 19–51.

[22]Aronson, D. A. G., Johansson, A. V., and Lofdahl, L., "Shear Free Turbulence near a Wall," *Journal of Fluid Mechanics*, Vol. 338, 1997, pp. 363–385.

[23]Hunt, J. C. R., "Turbulence Structure and Turbulent Diffusion Near Gas–Liquid Interfaces," *Gas Transfer at Water Surfaces*, edited by W. Brutsaert and G. H. Jirka, D. Reidel, Hingham, MA, 1984, pp. 67–82.

[24]Kevlahan, N. K.-R., and Hunt, J. C. R., "Non-Linear Interactions in Turbulence with Strong Irrotational Straining," *Journal of Fluid Mechanics*, Vol. 337m, 1997, pp. 333–364.

[25]Reynolds, A. J., and Tucker, H. J., "The Distortion of Turbulence by General Uniform Irrotational Strain," *Journal of Fluid Mechanics*, Vol. 68, 1975, pp. 673–693.

[26]Hoheisel, H., Kiock, R., Lichtfuss, H. J., and Fottner, L., "Influence of Free-stream Turbulence and Blade Pressure Gradient on Boundary Layer and Loss Behavior of Turbine Cascades," *Journal of Turbomachinery*, Vol. 109, April 1987, pp. 210–219.

[27]Krishnamoorthy, V., and Sukhatme, S. P., "The Effect of Free-Stream Turbulence on Gas Turbine Blade Heat Transfer," *Journal of Turbomachinery*, Vol. 111, Oct. 1989, pp. 497–501.

[28]Zhang, L., and Han, J.-C., "Combined Effect of Free-stream Turbulence and Unsteady Wake on Heat Transfer Coefficients from a Gas Turbine Blade," *Journal of Heat Transfer*, Vol. 117, May 1995, pp. 296–302.

[29]Hoffs, A., Drost, U., and Bolcs, A., "Heat Transfer Measurements on a Turbine Airfoil at Various Reynolds Numbers and Turbulence Intensities Including Effects of Surface Roughness," American Society of Mechanical Engineers, ASME Paper 96-GT-169, 1996.

[30]Ames, F. E., "The Influence of Large-Scale High-Intensity Turbulence on Vane Heat Transfer," *Journal of Turbomachinery*, Vol. 119, Jan. 1997, pp. 23–30.

[31]Gregory-Smith, D. G., and Cleak, J. G. E., "Secondary Flow Measurements in a Turbine Cascade with High Inlet Turbulence," *Journal of Turbomachinery*, Vol. 114, 1992, pp. 173–183.

[32]Hobson, G. V., and Shreve, R. P., "Inlet Turbulence Distortion and Viscous Flow Development in a Controlled Diffusion Cascade at Very High Incidence," *Journal of Propulsion and Power*, Vol. 9, No. 3, 1993, pp. 397–404.

[33]Wunderwald, D., and Fottner, L., "Experimental Investigation of Turbulence Structures in the Boundary Layer of a Highly Loaded Turbine Cascade," American Society of Mechanical Engineers, ASME Paper 96-GT-249, 1996.

[34]Bangert, B. A., Kohli, A., Sauer, J. H., and Thole, K. A., "High Freestream Turbulence Simulation in a Scaled Up Turbine Vane Passage," American Society of Mechanical Engineers, ASME Paper 97-GT-51, 1997.

[35]Ames, F. E., and Plesniak, M. W., "The Influence of Large-Scale High-Intensity Turbulence on Vane Aerodynamic Losses, Wake Growth and Exit Turbulence Parameters," *Journal of Turbomachinery*, Vol. 119, April 1997, pp. 182–192.

[36]de la Riva, D. H., "Turbulence Interaction in a Highly Staggered Cascade–Propulsor Configuration," M.S. Thesis, Dept. of Aerospace and Ocean Engineering, Virginia Polytechnic Inst. and State Univ., Blacksburg, VA, April 2001.

[37]Muthanna, C., "The Effects of Free Stream Turbulence on the Flow Field Through a Compressor Cascade," Ph.D. Dissertation, Dept. of Aerospace and Ocean Engineering, Virginia Polytechnic Inst. and State Univ., Blacksburg, VA, May 2002.

[38]Wang, Y., "Tip Leakage Flow Downstream a Compressor Cascade with Moving End Wall," M.S. Thesis, Dept. of Aerospace and Ocean Engineering, Virginia Polytechnic Inst. and State Univ., Blacksburg, VA, Feb. 2000.

[39]Muthanna, C., and Devenport, W. J., "The Wake of a Compressor Cascade With Tip Gap. Part 1. Mean Flow and Turbulence Structure," *AIAA Journal* (submitted for publication).

[40]Wang, Y., and Devenport, W. J., "The Wake of a Compressor Cascade With Tip Gap. Part 2. Effects of Endwall Motion," *AIAA Journal* (submitted for publication).

[41]Wenger, C. W., Devenport, W. J., Wittmer, K. S., and Muthanna, C., "The Wake of a Compressor Cascade With Tip Gap. Part 3. Two Point Statistics," *AIAA Journal* (submitted for publication).

[42]Wittmer, K. S., Devenport, W. J., and Zsoldos, J. S., "A Four Sensor Hot Wire Probe System for Three Component Velocity Measurements," *Experiments in Fluids*, Vol. 24, 1998, pp. 416–423; also Erratum, Vol. 27, No. 4, pp. U1, Sept. 1999.
[43]Bearman, P. W., "Corrections for the Effect of Ambient Temperature Drift on Hot-Wire Measurements in Incompressible Flow," *DISA Information*, No. 11, 1971, pp. 25–30.
[44]Comte-Bellot, G., and Corrsin, S., "The Use of a Contraction to Improve the Isotropy of Grid Generated Turbulence," *Journal of Fluid Mechanics*, Vol. 25, pp. 657–682.
[45]Pope, S. B., *Turbulent Flows*, Cambridge Univ. Press, New York, 2000.
[46]Hinze, J. O., *Turbulence*, McGraw–Hill, New York, 1975.
[47]Shin, S., "Reynolds-Averaged Navier–Stokes Computation of Tip Clearance Flow in a Compressor Cascade Using an Unstructured Grid," Ph.D. Dissertation, Dept. of Aerospace and Ocean Engineering, Virginia Polytechnic Inst. and State Univ., Blacksburg, VA, Sept. 2001.
[48]Goldstein, M. E., "Turbulence Generated by the Interaction of Entropy Fluctuations with Non-Uniform Mean Flows," *Journal of Fluid Mechanics*, Vol. 93, Pt. 2, 1979, pp. 209–224.

W. Dahm
*Associate Editor*